Imaging mantle plumes with instantaneous phase measurements of diffracted waves

Florian Rickers, Andreas Fichtner and Jeannot Trampert

Department of Earth Sciences, Utrecht University, Utrecht, the Netherlands; Email: rickers@geo.uu.nl

1. Introduction

Conclusive seismological evidence for the existence of mantle plumes is still missing and remains a challenge. Because plume conduits are supposedly smaller in diameter than the first Fresnel zone of teleseismic body waves, wavefront healing conceals travel time delays and hides mantle plumes from the tomographic eye.

In a synthetic tomographic experiment, we show that a misfit function based on simple cross-correlation travel times does not allow us to image a narrow plume conduit in the lower mantle. The reason is that cross-correlation measurements cannot capture details of the interference between direct and diffracted waves, which is essential in order to account for finite frequency effects.

The instantaneous phase difference, a 'full-waveform'-measurement, can capture these time-dependent variations. Due to its amplitude-independence, the instantaneous phase can furthermore measure low-amplitude diffracted waves in the P-wave coda. Using a misfit function based on the instantaneous phase difference of the P-wave window, we succeed to recover the same plume to greater depth than with simple travel time measurements. If we extend the measurement window further to take later-arriving diffracted waves into account, we fully recover the plume.

We conclude that the diffracted wavefield contains the necessary information to constrain mantle plumes with a diameter smaller than the width of the first Fresnel zone. The instantaneous phase difference is an ideal way to measure these diffracted waves.

2. The Model

The model extends 90° in the latitudinal and longitudinal directions, and 2500 km in depth. We use the spectral element code SES3D (Fichtner & Igel, 2008) to solve the elastic wave equation. The plume is implemented as a vertical cylinder of reduced P-wave velocity (-5% v_p with respect to PREM) and with a diameter of 300 km. The dominant P-wave period of the simulation is T=25 s, corresponding to a maximum width of the first Fresnel zone of $\approx$ 1400 km in the lower mantle. We use the dense station grid shown in Fig.2(a) to visualize spatial misfit distributions at the surface, and the setup in Fig. 2(b) to perform tomographic inversions.

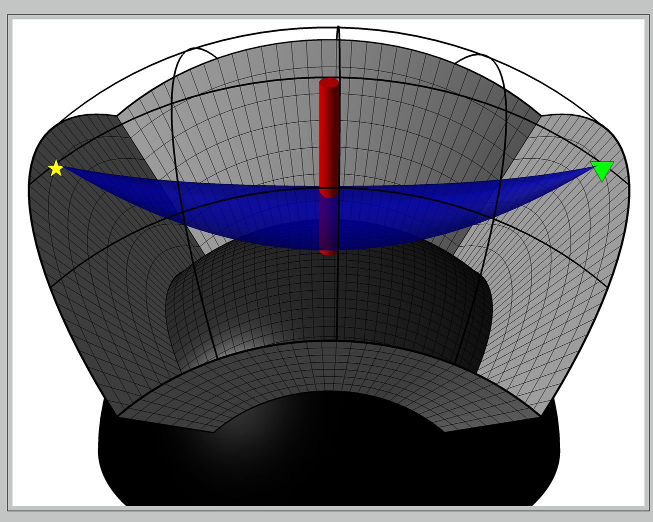

Figure 1: Setup of the experiment. The first Fresnel zone of the waves has a larger diameter than the plume conduit, resulting in strong finite-frequency effects.

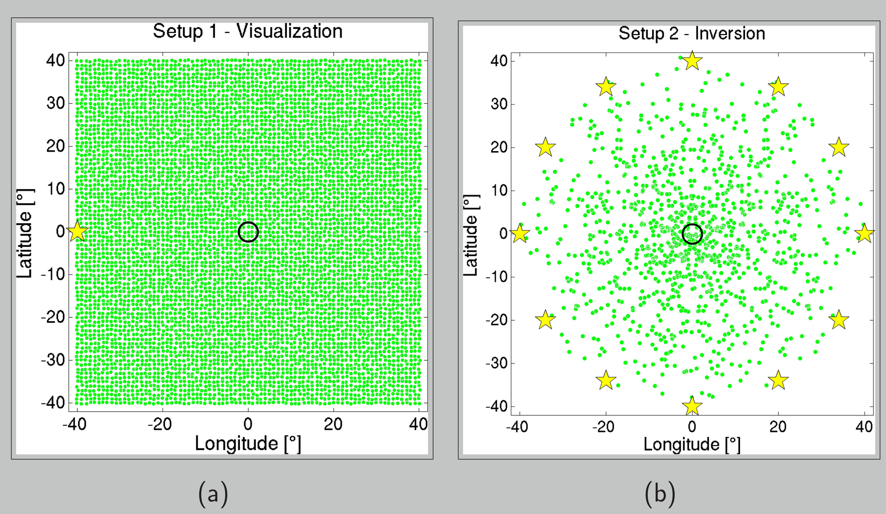

Figure 2: Location of events (red/yellow stars) and receivers (green dots) on the model surface. The black circle indicates the location of the plume. **(a)** Configuration for the visualization of the spatial misfit distribution. **(b)** Configuration for the tomographic inversions.

3. Misfit 1: Travel times

We measure travel time shifts by windowing the P-wave and cross-correlating the synthetic (PREM) and observed (PREM+plume) waveforms. The travel time shift corresponds to the time lag at the maximum of the cross-correlation function (Luo & Schuster, 1991).

Fig. 3(a) shows that wavefront healing reduces travel time delays already at short distances behind the plume. Fig. 3(b) shows a comparison of the measured travel time delays along the equator to the time delays that we would expect if ray theory was valid and measurements were not affected by wavefront healing.

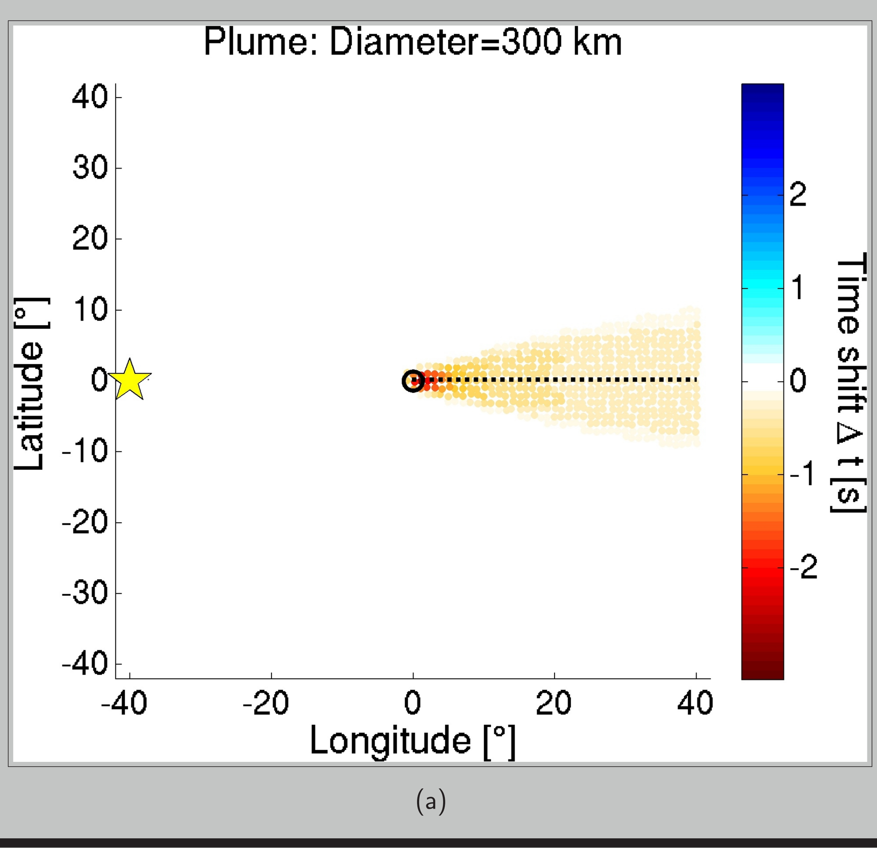

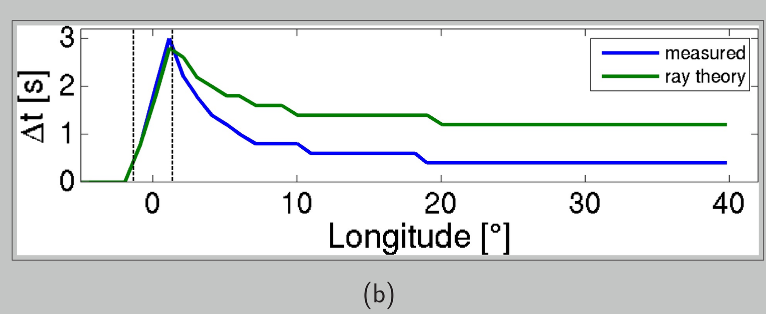

Figure 3: **(a)** Spatial distribution of P-wave cross-correlation travel time shifts at the surface. The dominant P-wave period is $T = 25$ s. The yellow star indicates the location of the source, the black circle is the plume with a diameter of 300 km. **(b)** Travel time shifts for receivers along the equator (indicated by the black dotted line in (a)). For comparison, expected ray-theoretical values are given.

We invert the travel time shifts using the source-receiver configuration in Fig. 2(b). We aim for a minimization of the misfit function

$$\chi(\mathbf{m}) = \sum_{i=1}^{N} [\Delta t_i(\mathbf{m})]^2, \tag{1}$$

with N being the total number of receivers, Δt_i the P-wave travel time delay at receiver i and $\mathbf{m}$ the current model. We use an iterative conjugate gradient scheme and compute the gradient of the misfit function using adjoint methods, thereby taking into account the finite-frequency nature of seismic waves in the forward as well as in the inverse problem. We end the iterations when the value of the misfit function is reduced by 95% with respect to the initial value.

The resulting tomographic model is presented in Fig. 4(b), next to the original plume in Fig. 4(a) which we used to generate the data. While the upper mantle part of the plume is imaged reasonably well, the lower mantle part remains largely unconstrained. The measured travel time shifts do not contain sufficient information to constrain the lower mantle part of the plume. The width of the first Fresnel zone limits the tomographic resolution when travel times are used, those parts of the plume that are considerably smaller than the first Fresnel zone are not well-constrained.

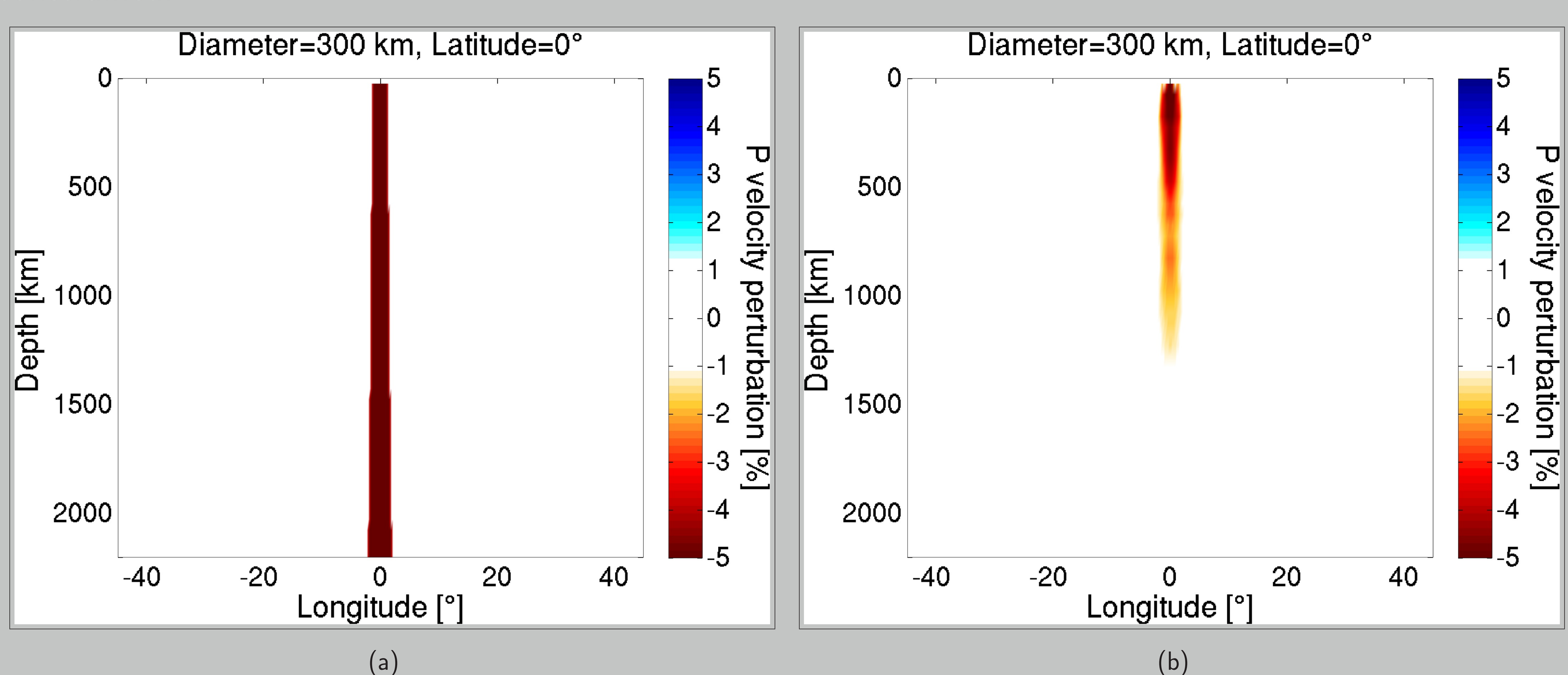

Figure 4: **(a)** Original plume **(b)** Recovered plume using cross-correlation travel time shifts.

4. Misfit 2: Instantaneous phase difference

The instantaneous phase (Bozdağ *et al.*, 2011) assigns a time-dependent phase $\phi(t)$ to a time series $u(t)$ at every instant in time, making use of the analytical signal

$$a(t) = u(t) - iH\left[u(t)\right], \tag{2}$$

with $H[u(t)]$ being the Hilbert transform of $u(t)$. The analytical signal $a(t)$ can be written in exponential form, providing a natural separation of the signal into 'instantaneous amplitude' $A(t)$ and 'instantaneous phase' $\phi(t)$:

$$a(t) = A(t)e^{i\phi(t)}. \tag{3}$$

As we are interested in the phase difference between two time series $u_1(t)$ and $u_2(t)$, we multiply one of the analytical signals with the complex conjugate of the other:

$$c(t) = a_1^*(t)a_2(t) = A_1(t)A_2(t)e^{i[\phi_2(t)-\phi_1(t)]} \tag{4}$$

We can then compute the instantaneous phase difference through:

$$\Delta\phi(t) = \tan^{-1}\frac{\mathrm{Im}[c(t)]}{\mathrm{Re}[c(t)]} \tag{5}$$

In practice it is necessary to regularize the instantaneous phase difference in order to prevent cycle slips in low amplitude parts of the signal. This is a quite sensitive process and can be achieved by defining a treshold based on the instantaneous amplitude.

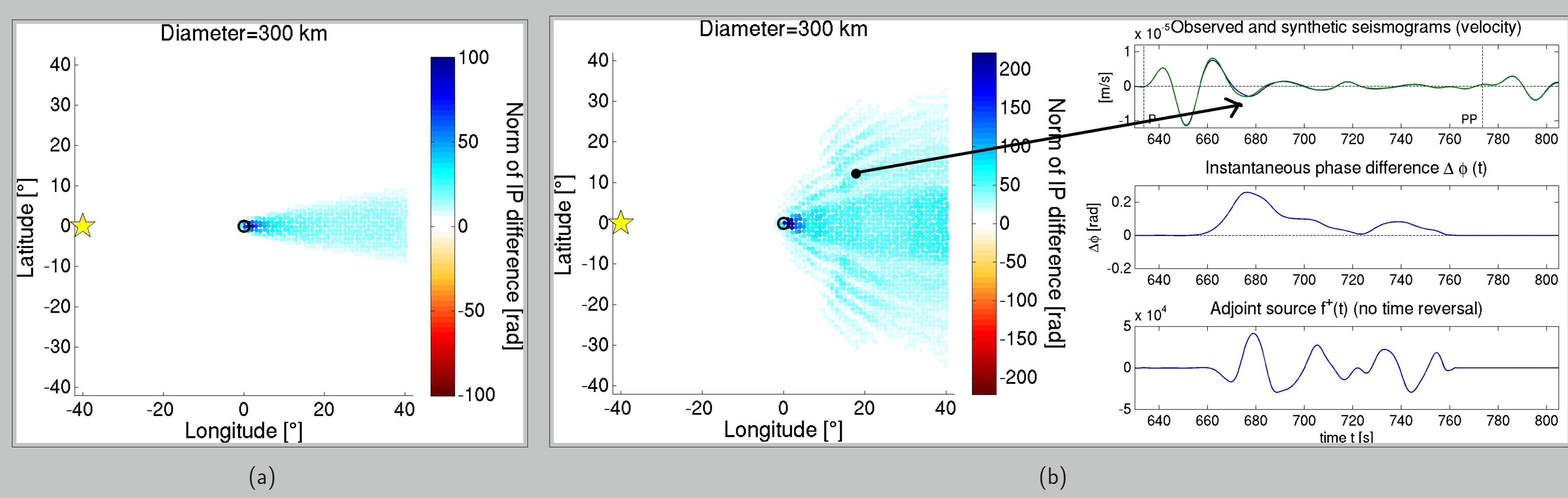

Figure 5: Spatial distribution of the L_2-norm of the instantaneous difference $||\Delta\phi(t)||$, measured using the dense station network in Fig. 1(b). **(a)** for the same P-wave window as in the cross-correlation case. **(b)** for an extended P-wave window, reaching up to the onset of the PP-wave. An example of an instantaneous phase measurement of a later-arriving diffracted wave is given.

Fig. 4(a) shows that the L_2-norm of the instantaneous phase difference has a similar distribution over the model surface as the cross-correlation measurement in Fig. 3(a) does, when we measure over the P-wave window only. Because the instantaneous phase difference is an amplitude-independent measurement, we can extend the window and include the P-wave coda in the measurement, as is shown in Fig. 4(b). Despite their low amplitude, phase differences in the coda contribute to the measurement with an equal weight as the main phase does. This enables us to measure later-arriving diffracted waves. Using this additional information in an inversion helps in constraining the plume better at depth.

The inversion technique is identical to the travel time based case, with the difference that we now minimize a misfit function based on the instantaneous phase difference $\Delta\phi(t)$:

$$\chi(\mathbf{m}) = \sum_{i=1}^{N} [\Delta\phi_i(t,\mathbf{m})]^2. \tag{6}$$

We perform one inversion using the window of the P-wave only, and a second inversion using the extended P-wave window which includes the coda of the P-wave. The resulting tomographic model in Fig. 6(a) shows that the plume is already constrained to greater depth if we use the P-wave window only. The extension of the measurement window to cover more of the diffracted wavefield results in an almost complete recovery of the plume (Fig. 6(b)). We conclude that the necessary information to constrain a narrow plume conduit below the size of the first Fresnel zone is contained within the diffracted wavefield. By measuring these diffracted waves and inverting this information, lower mantle plumes can be constrained even at depth.

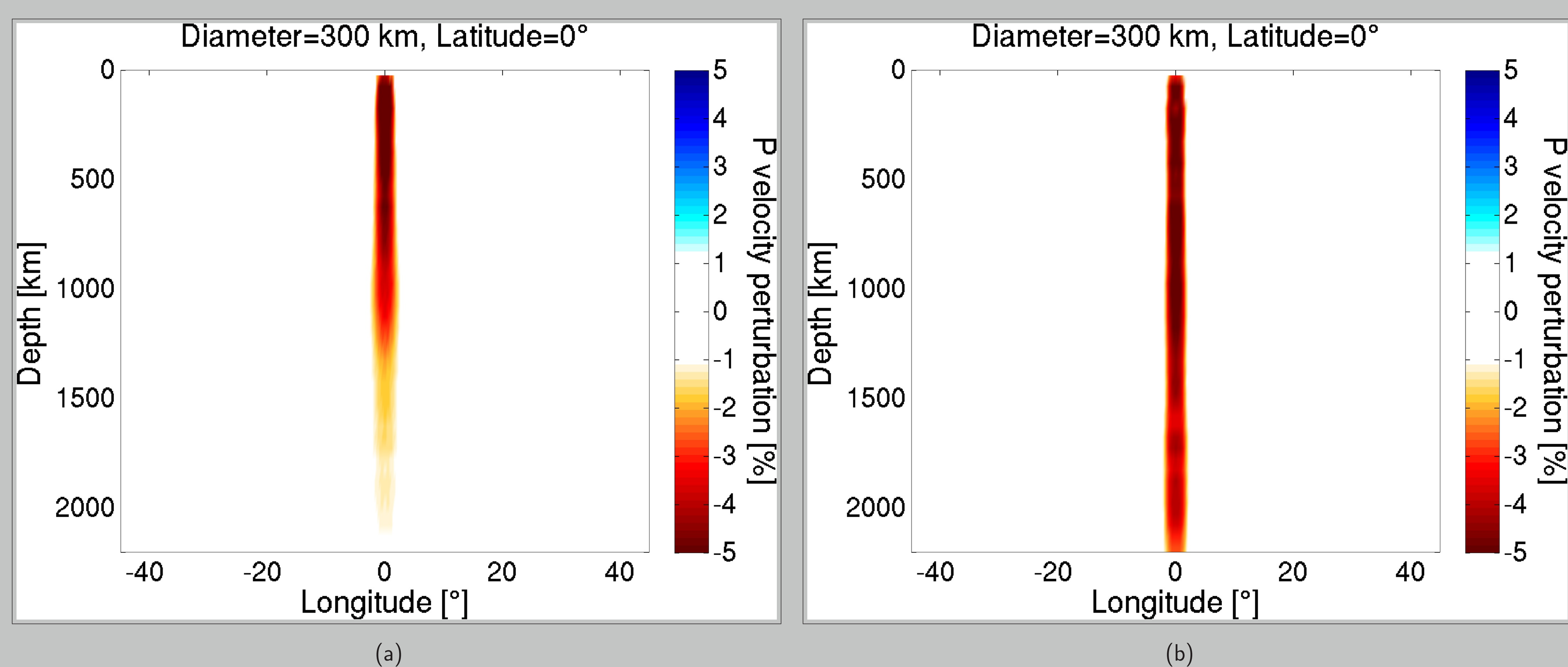

Figure 6: **(a)** Recovered plume using the instantaneous phase difference of the P-wave window. **(b)** Recovered plume using the instantaneous phase difference of the extended P-wave window which includes more of the diffracted wavefield.

5. Conclusions

- Lower mantle plumes with a size considerably smaller than the first Fresnel zone cannot be imaged when cross-correlation travel time delays are used.
- The use of finite-frequency sensitivity kernels alone does not account for wavefront healing in an inversion.
- The instantaneous phase difference captures the time-dependent interaction between direct and diffracted waves and allows for the measurement of small-amplitude diffracted waves.
- We can obtain a better tomographic image of a narrow plume by using the instantaneous phase difference of the P-wave window. If we extend the measurement window to include the diffracted waves in the P-wave coda, we can recover the plume fully.
- The time-dependent measurement of diffracted waves which arrive later than the main phase yields the necessary information to constrain narrow mantle plumes even at depth.

6. References

Bozdağ, E., Trampert, J. & Tromp, J., 2011. Misfit functions for full waveform inversion based on instantaneous phase and envelope measurements. *Geophys. J. Int.*, **185**, 845–870.

Fichtner, A. & Igel, H., 2008. Efficient numerical surface wave propagation through the optimization of discrete crustal models - a technique based on non-linear dispersion curve matching. *Geophys. J. Int.*, **173**, 519–533.

Luo, Y. & Schuster, G. T., 1991. Wave-equation traveltime inversion. *Geophysics*, **56**, 645–653.